

Article

Synergistic Action of Biosynthesized Silver Nanoparticles and Culture Supernatant of *Bacillus amyloliquefacience* against the Soft Rot Pathogen *Dickeya dadantii*

Afsana Hossain ^{1,2,3}, Jinyan Luo ^{4,*}, Md. Arshad Ali ², Rongyao Chai ¹, Muhammad Shahid ⁵,
Temoor Ahmed ², Mohamed M. Hassan ⁶, Roqayah H. Kadi ⁷, Qianli An ², Bin Li ² and Yanli Wang ^{1,*}

- ¹ State Key Laboratory for Quality and Safety of Agro-Products, Institute of Plant Protection and Microbiology, Zhejiang Academy of Agricultural Sciences, Hangzhou 310021, China; afsana_07@yahoo.com (A.H.); rychai@sina.com (R.C.)
- ² Institute of Biotechnology, Zhejiang University, Hangzhou 310058, China; alibau201@gmail.com (M.A.A.)
- ³ Department of Plant Pathology, Bangabandhu Sheikh Mujibur Rahman Agricultural University, Gazipur 1706, Bangladesh
- ⁴ Department of Plant Quarantine, Shanghai Extension and Service Center of Agriculture Technology, Shanghai 201103, China
- ⁵ Department of Bioinformatics and Biotechnology, Government College University, Faisalabad 38000, Pakistan
- ⁶ Department of Biology, College of Science, Taif University, Taif 21944, Saudi Arabia
- ⁷ Department of Biology, Faculty of Science, University of Jeddah, Jeddah 21959, Saudi Arabia
- * Correspondence: toyanzi@126.com (J.L.); ylwang88@aliyun.com (Y.W.)

Abstract: Nanomaterials are increasingly being used for crop growth, especially as a new paradigm for plant disease management. Among the other nanomaterials, silver nanoparticles (AgNPs) draw a great deal of attention because of their unique features and multiple usages. Rapid expansion in nanotechnology and utilization of AgNPs in a large range of areas resulted in the substantial release of these nanoparticles into the soil and water environment, causing concern for the safety of ecosystems and phytosanitary. In an attempt to find an effective control measure for sweet potato soft rot disease, the pathogen *Dickeya dadantii* was exposed to AgNPs, the cell-free culture supernatant (CFCS) of *Bacillus amyloliquefaciens* alone, and both in combination. AgNPs were synthesized using CFCS of *Bacillus amyloliquefaciens* strain A3. The green synthesized AgNPs exhibited a characteristic surface plasmon resonance peak at 410–420 nm. Electron microscopy and X-ray diffraction spectroscopy determined the nanocrystalline nature and 20–100 nm diameters of AgNPs. Release of metal Ag⁺ ion from biosynthesized AgNPs increases with time. AgNPs and CFCS of *B. amyloliquefaciens* alone exhibited antibacterial activity against the growth, biofilm formation, swimming motility, and virulence of strain A3. The antibacterial activities elevated with the elevation in AgNPs and CFCS concentration. Similar antibacterial activities against *D. dadantii* were obtained with AgNPs at 50 µg·mL⁻¹, 50% CFCS alone, and the combination of AgNPs at 12 µg·mL⁻¹ and 12% CFCS of *B. amyloliquefaciens*. In planta experiments indicated that all the treatments reduced *D. dadantii* infection and increased plant growth. These findings suggest that AgNPs along with CFCS of *B. amyloliquefaciens* can be applied to minimize this bacterial disease by controlling pathogen-contaminated sweet potato tuber with minimum Ag nano-pollutant in the environment.

Keywords: silver nanoparticles; synergistic action; *Dickeya dadantii*; sweet potato



Citation: Hossain, A.; Luo, J.; Ali, M.A.; Chai, R.; Shahid, M.; Ahmed, T.; M. Hassan, M.; H. Kadi, R.; An, Q.; Li, B.; et al. Synergistic Action of Biosynthesized Silver Nanoparticles and Culture Supernatant of *Bacillus amyloliquefacience* against the Soft Rot Pathogen *Dickeya dadantii*. *Plants* **2023**, *12*, 1817. <https://doi.org/10.3390/plants12091817>

Academic Editor: Kwang-Hyun Baek

Received: 31 March 2023

Revised: 21 April 2023

Accepted: 25 April 2023

Published: 28 April 2023



Copyright: © 2023 by the authors. Licensee MDPI, Basel, Switzerland. This article is an open access article distributed under the terms and conditions of the Creative Commons Attribution (CC BY) license (<https://creativecommons.org/licenses/by/4.0/>).

1. Introduction

The application of nanoscale-size materials possessing no less than one dimension in the 1 to 100 nanometers range is a newly emerging area in nanoscience and technology. The nanomaterials display exceptional physical, chemical, and electrical properties for their extreme surface-to-volume ratio [1]. The extensive use of nanoparticles raises concern about their environmental impact, but the impact of NPs on ecological processes and organisms

remains largely unknown. Enormous production and application of NPs release nano-size materials into the environment during the production process as well as using, and these NPs have an unknown consequence on ecosystem structure and functioning when they enter aquatic and terrestrial environmental processes [1,2].

Among the diverse types of metal nanoparticles, silver nanoparticles gained boundless attention for application in multiple disciplines, especially in the agricultural field, because of their exclusive properties such as chemical stability, good conductivity, catalytic, and, most importantly, antimicrobial activities [3–5]. Silver nanoparticles exhibit antibacterial activity using different mechanisms, although these mechanisms have yet to be fully elucidated. Many studies state that AgNPs can disrupt the cell wall; increase intercellular ROS production, oxidative stress, and photocatalytic activity; and inhibit cell division and replication by binding to cell walls, the S-H group of proteins, and the N7 atom of guanine [6,7]. Green synthesis of silver nanoparticles attained worldwide attention due to their minimum use of resources and energy as well as for their biocompatibility and environmental safety [8,9]. The growing use of AgNPs inevitably increases the chance of releasing toxic Ag^+ into the environment. Research showed that AgNPs at any level of concentration caused oxidative stress and serious inhibition of photosynthesis, which ultimately retarded the growth of plants and exhibited higher toxicity [10,11].

Gram-positive bacteria belonging to the genera *Bacillus* are found in nature and inhibit other pathogenic microorganisms present in the rhizosphere and seeds. They are an effective and eco-friendly method for the biological control of a large number of plant fungal and bacterial diseases [12,13]. *Bacillus* spp. are the best candidates for producing effective biopesticides because of their spore-forming ability and resistance to dryness [14]. *Bacillus* can produce a vast array of biologically active molecules, such as non-ribosomally synthesized peptides and lipopeptides, polyketides, bacteriocins, and siderophores, that are important and can potentially inhibit phytopathogenic bacteria [14,15]. Studies have shown that lipopeptides present in the culture filtrate of *Bacillus* have biocontrol capacity against fungus and bacteria [15–17].

The control of bacterial disease mostly relies on chemical pesticides. The broad-spectrum use of chemical pesticides has resulted in the development of multi-drug resistant bacteria, which is a main threat to controlling bacterial infection. Limiting the chemical pesticide application rate in agriculture is one of the main objectives for current agricultural production. This can be achieved in diverse ways, either by introducing new or more effective alternatives, such as nanoparticles, or by the combination of nanoparticles with other effective alternatives, such as plant extracts or culture filtrates of antagonistic fungi and bacteria. The use of AgNPs combined with culture filtrate may become a popular alternative as this method reduces the risk of hazardous Ag^+ . The combination of two or more tested materials can reduce the amount of Ag^+ needed to control pathogens and the negative consequences of AgNPs on human health and nature [1,18]. Therefore, the control of bacterial pathogens using biosynthesized nanoparticles and *Bacillus* can be an effective alternative to chemical pesticides [7,19].

Gram-negative bacteria from the genera of *Pectobacterium* and *Dickeya* [20] are broad-host-range pathogens, which can attack many crop and ornamental plants [21]. They are causative agents of destructive soft rot disease for various vegetable and ornamental plants due to the production of pectinase, which can degrade pectin in the primary walls and middle lamella of plant cell walls, resulting in plant tissue maceration [22,23]. Over the last two decades, foot rot in rice [24,25], stalk rot in maize [26], black leg and soft rot in potato [27–29], stem and root rot in sweet potato [30,31], and soft rot and sheath rot in banana [32,33] caused by some aggressive species of *Dickeya* have hampered staple food security. Few crop varieties are resistant to *Dickeya* and *Pectobacterium*, while the control of soft rot in agricultural fields is highly dependent on effective antibiotic use, which will not be feasible in the future because of the threat of environmental pollution and antibiotic-resistant human and animal pathogens. However, the increased consumer demand for chemical-free foods has motivated researchers to find promising prevention

and control strategies that can serve as alternatives to chemical pesticides. Antagonistic *Bacillus*, *Paenibacillus* biosynthesized AgNPs, ZnONPs, and TiO₂NPs can potentially inhibit *Dickeya dadantii* causing stem and root rot on sweet potato [34–36].

Recently, *Dickeya dadantii* soft rot was found in most sweet potato growing areas in China, indicating a need for an efficient strategy to control this pathogen. The objective of this study was to determine the potentiality of the combination of CFCS and AgNPs against *D. dadantii*.

2. Results and Discussion

In our previous study [37], the in vivo and in vitro antibacterial activity of 21 different *Bacillus* strains were screened against *D. dadantii*. Among all *Bacillus* strains, *B. amyloliquefaciens* A3 showed significantly higher antibacterial activity against *D. dadantii* compared to other *Bacillus* strains. Furthermore, silver nanoparticles were successfully synthesized using the cell-free culture supernatant of *B. amyloliquefaciens* A3 with the incubation of silver nitrate [35,38].

2.1. Characterization of Synthesized AgNPs with *B. amyloliquefaciens* CFCS

AgNPs were synthesized by incubating the CFCS of *B. amyloliquefaciens* and AgNO₃ (3 mM). After 48 h, the mixture changed to a dark brown color from light yellow, which indicated the reduction of Ag⁺ into Ag⁰ in AgNO₃ solutions. UV-Vis spectrometry confirmed the existence of synthesized AgNPs in the solution [39], which showed a characteristic surface plasmon resonance peak at 410–420 nm (Figure 1a). Previous studies showed that free electrons of silver nanoparticles exhibited surface plasmon resonance at 410 to 450 nm [38,40–42].

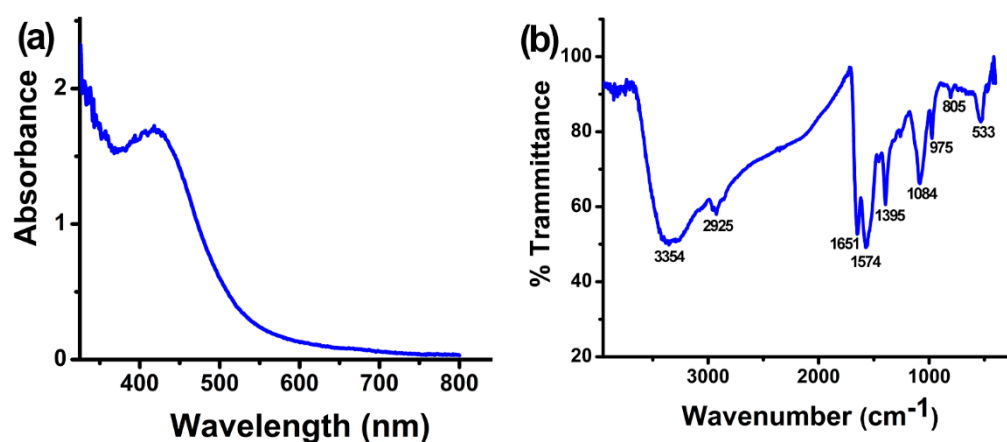


Figure 1. Characterization of cell-free culture supernatant (CFCS) of *Bacillus amyloliquefaciens* mediated silver nanoparticles (a) Ultra violet-visible spectrum of newly synthesized AgNPs solution. Synthesized AgNPs exhibit a clear surface plasmon resonance peak at 410–420 nm. (b) Fourier transform infrared spectrum displaying functional group accountable for the AgNPs synthesis and their stabilization.

FTIR spectrometry revealed the functional groups in the CFCS of *B. amyloliquefaciens* A3 that cause the reduction of Ag⁺, stabilization, and AgNPs capping. The FTIR spectrum of the synthesized AgNPs exhibited absorption peaks at 3354, 2925, 1651, 1574, 1395, 1084, 975, 805, and 533 cm⁻¹ (Figure 1b). The peak at 3354 cm⁻¹ is for N–H stretching vibration; the peak at 2925 cm⁻¹ corresponds to C–H stretching vibration and N–H stretching of the amide group; the peak at 1651 cm⁻¹ corresponds to C=O and C=C stretching vibrations; the band at 1574 cm⁻¹ is attributed to C=C stretching vibration; the peak at 1395 cm⁻¹ is attributed to CH₃ or C–H bending; the peak at 975 cm⁻¹ corresponds to C=C bending and C–H vibration; and the peaks at 1084 cm⁻¹, 805 cm⁻¹, and 533 cm⁻¹ are for C=O stretching, C–H bending, and C–C skeleton vibration, respectively. The existence of these

functional groups confirmed the presence of protein in the CFCS of *B. amyloliquefaciens* and also indicated that these groups act as reducing and stabilizing agents in the synthesis process of AgNPs [43,44]. Earlier reports showed that free amine groups as well as cysteine residue in proteins can combine with nanoparticles and stabilize the AgNPs [45].

The X-ray diffraction patterns revealed the nanocrystalline nature of synthesized AgNPs. Based on the Bragg reflection peak at 2θ , the values of 27.86, 32.27, 46.22, 54.86, and 76.74 correspond to planes (101), (111), (200), (220), and (311), respectively (Figure 2a). The four reflection peaks are correlated with the crystallographic nature of the centering face and the cubic nature of AgNPs, which was confirmed with a comparison to the powder diffraction card of the Joint Committee on Powder Diffraction Standard File No. JCPDS 04-0783. The average particle diameter of AgNPs is 50.3 nm, which was calculated using the Debye–Scherrer equation:

$$D = K\lambda / (\beta \cos\theta),$$

where D represents the median crystalline nanoparticles size, K (0.94) represents the Scherrer constant, λ (0.15406 nm) represents the wavelength of X-ray, β represents the full breadth at half largest of the X-ray diffraction peak, and θ represents the Bragg angle.

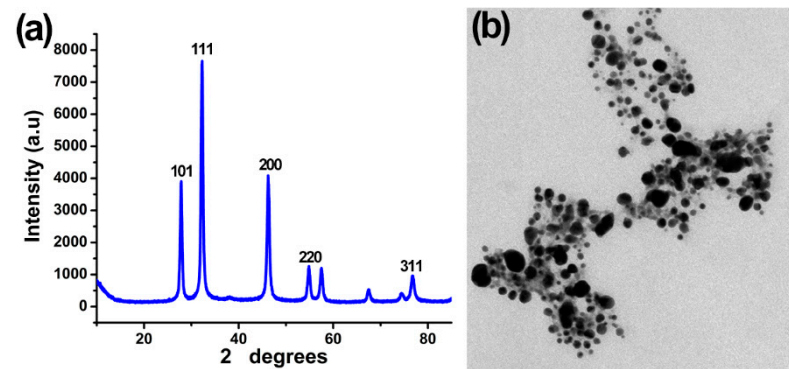


Figure 2. Characterization of cell-free culture supernatant (CFCS) of *Bacillus amyloliquefaciens* mediated silver nanoparticles (a) X-ray diffraction spectrum demonstrating the nanosize and crystalline nature of the AgNPs (b) TEM displaying AgNPs with a diameter of 20–100 nm and spherical form.

Transmission (TEM) electron microscopy and scanning (SEM) electron microscopy were used to confirm the AgNP sizes that were synthesized from the CFCS of *B. amyloliquefaciens*. The TEM images (Figure 2b) showed that most of the AgNPs had uniform size, were mono-dispersed, and about 20–100 nm in diameter with spherical shape and an average mean size of 48.5 nm, which were confirmed with the SEM images (Figure 3a). These results are consistent with previous studies [35,43].

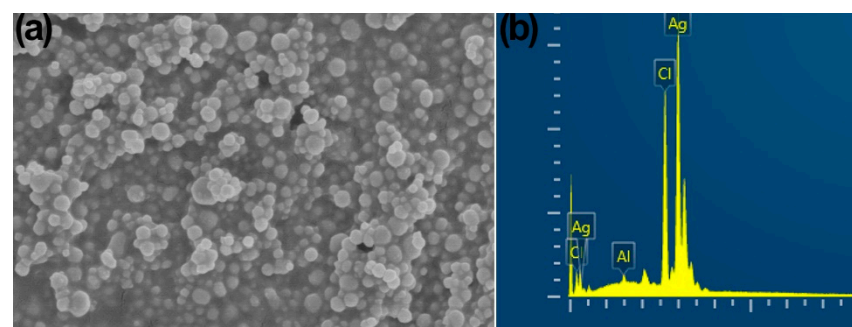


Figure 3. Characterization of cell-free culture supernatant (CFCS) of *Bacillus amyloliquefaciens* mediated silver nanoparticles (a) SEM displaying AgNPs with a diameter of 20–100 nm and spherical form. (b) Energy dispersive spectrum displaying the prevalence of Ag element in the AgNPs.

Energy dispersive spectroscopy further confirmed the dominance of metal silver (Ag^0) in the synthesized AgNPs. The typical absorption peak of the Ag element was exhibited by AgNPs at 3 KeV (Figure 3b), which confirmed that nano-sized silver was in a pure form, as earlier reports have shown [35,38,41,46–48]. Spectroscopy showed 82.32 wt% Ag^0 along with 17.07 and 0.61 wt% of Cl and Al, respectively.

2.2. Metal Ag Release

The metal release data indicated that biosynthesized AgNPs significantly release Ag^+ ions in ddH₂O during every time interval (Figure 4). After 8 h, a quick initial release of Ag^+ ions from the biosynthesized AgNPs was observed, which then attained a persistent value. Biosynthesized AgNPs released the most Ag^+ (2.25) after 24 h. Previous studies found that there is a correlation between the suppression of disease and the ion release profile [49]. Moreover, components of different media have a specific function in releasing metal ions from nanoparticles.

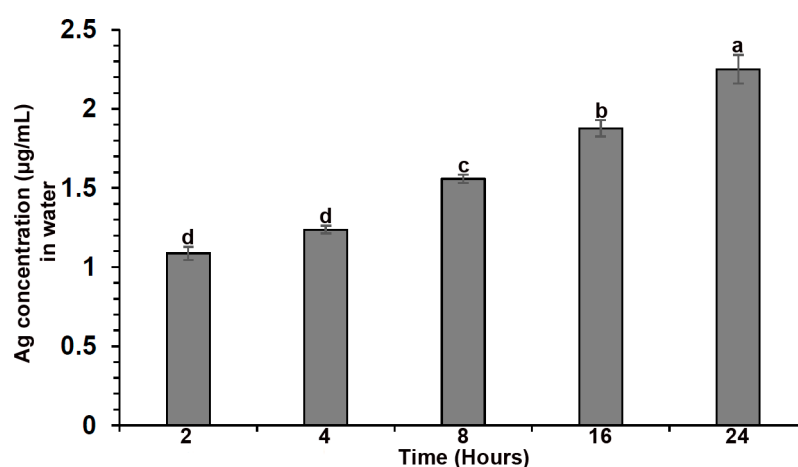


Figure 4. Release of Ag^+ ions during different time intervals. Different lowercase letters on the bars are represented the significantly different at $p \leq 0.05$.

2.3. Antibacterial Activity of the Combination of CFCS and AgNPs against *D. dadantii*

AgNPs (50 μL), CFCS (50%), and the combination of AgNPs (12 μL) and CFCS (12%) exhibit a similar extended of inhibition of growth and swimming motility against *D. dadantii* strain A3 and tissue maceration in sweet potato. The inhibition of in vivo tissue maceration using tuber slices was in general agreement with the result of in vitro bacterial growth, biofilm formation, and swimming motility.

AgNPs synthesized with *B. amyloliquefaciens* at different concentrations (12, 24, and 50 μL) and the CFCS of *B. amyloliquefaciens* at different percentage (12, 24, and 50%) can significantly inhibit *D. dadantii* growth in liquid broth. Inhibition increases with the increase in concentration of AgNPs or percentage of CFCS (Tables 1 and 2). The highest inhibition of *D. dadantii* growth was found using 50 μL AgNPs and 50% CFCS. The combination of AgNPs (12 μL) and CFCS (12%) can significantly inhibit *D. dadantii* growth at a similar extent as 50 μL AgNPs and 50% CFCS (Table 3).

Table 1. Growth of *D. dadantii* in liquid nutrient broth containing CFCS (12, 25, or 50%) corresponded to an optical density at 600 nm (OD_{600}).

Treatment	Value at OD_{600}
<i>D. dadantii</i>	1.01 ± 0.02 d
<i>D. dadantii</i> + 12%	0.59 ± 0.03 c
<i>D. dadantii</i> + 25%	0.34 ± 0.03 b
<i>D. dadantii</i> + 50%	0.13 ± 0.02 a

Different letters within the same column indicate a statistically significant difference ($p < 0.05$).

Table 2. Growth of *D. dadantii* in liquid nutrient broth containing AgNPs (12, 25, or 50 $\mu\text{g}\cdot\text{mL}^{-1}$) corresponding to an optical density at 600 nm.

Treatment	Value at OD ₆₀₀
<i>D. dadantii</i>	1.02 ± 0.03 d
<i>D. dadantii</i> + AgNPs (12 μg)	0.44 ± 0.03 c
<i>D. dadantii</i> + AgNPs (25 μg)	0.33 ± 0.02 b
<i>D. dadantii</i> + AgNPs (50 μg)	0.12 ± 0.02 a

Different letters within the same column indicate a statistically significant difference ($p < 0.05$).

Table 3. Growth of *D. dadantii* in liquid nutrient broth containing CFCS (50%), AgNPs (50 $\mu\text{g}\cdot\text{mL}^{-1}$), and the combination of CFCS (12%) and AgNPs (12 $\mu\text{g}\cdot\text{mL}^{-1}$) corresponding to an optical density at 600 nm.

Treatment	Value at OD ₆₀₀
<i>D. dadantii</i>	1.04 ± 0.03 b
<i>D. dadantii</i> + CFCS (50%)	0.13 ± 0.02 a
<i>D. dadantii</i> + AgNPs (50 μg)	0.12 ± 0.02 a
<i>D. dadantii</i> + CFCS (12%) + AgNPs (12 μg)	0.11 ± 0.02 a

Different letters within the same column indicate a statistically significant difference ($p < 0.05$).

After 24 h of incubation at 30 °C without shaking, *D. dadantii* formed biofilm on the surface of the polystyrene plate. The combination of AgNPs (12 μL) and CFCS (12%) significantly inhibited (72%) the formation of biofilm, whereas AgNPs (50 μL) and CFCS (50%) alone showed a similar extent of inhibition (Table 4).

Table 4. Biofilm formation, swimming motility of *D. dadantii*, and the diameter of macerated tissue generated by *D. dadantii* in sweet potato tuber slices with CFCS (50%), AgNPs (50 $\mu\text{g}\cdot\text{mL}^{-1}$), and the combination of CFCS (12%) and AgNPs (12 $\mu\text{g}\cdot\text{mL}^{-1}$).

Treatment	Value at OD ₅₇₀	Colony Diameter (mm)	Tissue Maceration (mm)
<i>D. dadantii</i>	0.187 ± 0.04 b	30.70 ± 1.00 b	34.95 ± 0.79 b
<i>D. dadantii</i> + CFCS (50%)	0.062 ± 0.04 a	13.52 ± 0.84 a	13.20 ± 1.25 a
<i>D. dadantii</i> + AgNPs (50 μg)	0.055 ± 0.04 a	12.38 ± 0.83 a	12.13 ± 0.98 a
<i>D. dadantii</i> + CFCS (12%) + AgNPs (12 μg)	0.051 ± 0.04 a	10.03 ± 0.89 a	11.10 ± 0.94 a

Different letters within the same column indicate a statistically significant difference ($p < 0.05$).

Dickeya dadantii grew and showed swimming ability in semi-solid media with 0.3% (w/v) agar and formed a 35 mm diameter halo after 48 h of incubation at 30 °C (Table 4). The combination of AgNPs (12 μL) and CFCS (12%) significantly inhibited (68%) the halo diameter, whereas AgNPs (50 μL) and CFCS (50%) alone showed a similar extent of inhibition.

In sweet potato tubers, *D. dadantii* created a maceration zone by degrading plant cell walls in the sweet potato slice. One day after inoculation, the maceration zone was about 32 mm (Table 4). The combination of AgNPs (12 μL) and CFCS (12%) significantly inhibited (65%) tissue maceration, whereas AgNPs (50 μL) and CFCS (50%) alone showed a similar extent of inhibition.

TEM also revealed the morphological changes in *D. dadantii* cells after treatment with the combination of AgNPs (12 μL) and CFCS (12%). After 4 h of treatment, most *D. dadantii* cells were dead, as indicated by distorted cells with disintegrated cytoplasm and cell walls (Figure 5c,d). On the other hand, *D. dadantii* cells grown without treatment had intact cell walls with dense cytoplasm filled in the cell (Figure 5a,b).

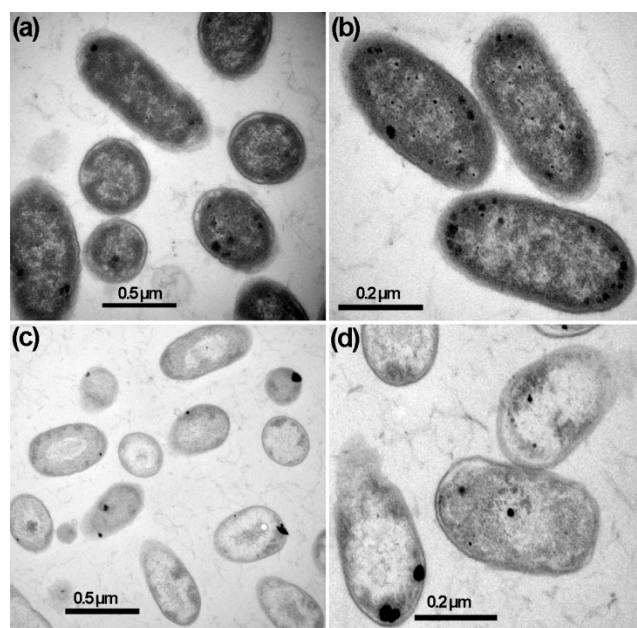


Figure 5. Transmission electron micrograph (TEM) images showing *Dickeya dadantii* cells without treatment (a,b) and those treated with the combination of silver nanoparticles (12 µL) and cell-free culture supernatant (12%) (c,d). Intact cell walls and dense cytoplasm characterized the control cells without treatment (a,b). Disintegration and clearing of the cytoplasm were evident in cells after 4 h of treatment (c,d).

During the in planta experiment, *D. dadantii* was inoculated into sweet potato seed tubers, and due to the infection, the tubers became rotten. *D. dadantii* was then recovered from the rotten inoculated tubers. Seed tubers treated with water germinated and became small seedlings 21 days post-inoculation. On the other hand, seed tubers treated with AgNPs (50 µg·mL⁻¹) from the CFCS of *B. amyloliquefaciens* A3, the CFCS of *B. amyloliquefaciens* A3 (50%), and the combination of AgNPs (12 µg·mL⁻¹) and CFCS (12%) germinated and became seedlings with a greater height than the seedlings grown from the water-treated seed tubers (Table 5). The fresh weight and dry weight of seedlings grown from sweet potato seed tubers treated with AgNPs (50 µg·mL⁻¹) from the CFCS of *B. amyloliquefaciens* A3, the CFCS of *B. amyloliquefaciens* A3 (50%), and the combination of AgNPs (12 µg·mL⁻¹) and CFCS (12%) were higher than the fresh and dry weight of the seedlings grown from water-treated seed tubers (Table 5).

Table 5. Seedling height, fresh and dry weight of seedlings raised from sweet potato seed tubers treated with water, *D. dadantii*, *D. dadantii* with the CFCS of *B. amyloliquefaciens* A3 (50%), AgNPs (50 µg·mL⁻¹) from the CFCS of *B. amyloliquefaciens* A3, or the combination of AgNPs (12 µg·mL⁻¹) and CFCS (12%).

Treatment	Seedling Height (cm)	Fresh Weight (gm)	Dry Weight (gm)
Water	2.5 ± 0.09 b	0.29 ± 0.04 b	0.04 ± 0.01 b
<i>D. dadantii</i>	0.0 ± 0.00 c	0.00 ± 0.00 c	0.00 ± 0.00 c
<i>D. dadantii</i> + CFCS (50%)	6.3 ± 0.22 a	0.73 ± 0.04 a	0.13 ± 0.02 a
<i>D. dadantii</i> + AgNPs (50 µg)	6.2 ± 0.27 a	0.71 ± 0.03 a	0.10 ± 0.01 a
<i>D. dadantii</i> + CFCS (12%) + AgNPs (12 µg)	6.6 ± 0.27 a	0.76 ± 0.04 a	0.14 ± 0.02 a

Different letters within the same column indicate a statistically significant difference ($p < 0.05$).

AgNPs may transport Ag⁺ more efficiently to the bacterial membrane and cytoplasm [50]. Ag⁺ release from the 20–80 nm silver nanoparticle and subsequent pene-

tration to the bacterial cell membrane might be the primary cause for the antibacterial action of AgNPs [50–53]. The CFCS of *B. amyloliquefaciens*-derived AgNPs were about 20–100 nm in width and inhibited the growth, biofilm formation, and swimming motility of *D. dadantii* through attachment to surfaces of bacterial cells, which may release toxic Ag⁺ and damage the cell membrane. After penetration into the *D. dadantii* cells, AgNPs may generate oxidative stress and interact with the sulfur present in the membrane proteins and the phosphorous remaining in the DNA to disrupt the respiratory chain and cell division, which lead to cell death [53,54]. The antimicrobial actions of AgNPs are mainly due to the release of Ag⁺, and the release of Ag⁺ even in very low concentrations can account for the biological response [50].

On the other hand, *Bacillus* spp. are known to be active against a large range of phytopathogenic bacteria through competition with phytopathogens and antibiosis by producing antibiotics and metabolites. As a biocontrol agent, the main attribute of *Bacillus* spp. is their various secondary metabolites and capability to produce a wide range of structurally various antimicrobial substances [15]. In comparison with other isolates, 8% of the whole genome of plant-associated *B. amyloliquefaciens* strain FZB42 is involved in the production of secondary metabolites such as bacteriocins, antimicrobial peptides and lipopeptides, polyketides, and siderophore with microbial activities [55,56]. A higher concentration of surfactin was observed in the CFCS of *B. amyloliquefaciens* strain A3 among the effective strain against *D. dadantii* [37]. Surfactins belonging to lipopeptides with strong antibacterial activities [14,57] may play a key role in the inhibition of growth and biofilm formation of *D. dadantii*. Previous studies showed that silver nanoparticles synthesized with the incubation of the CFCS of *Bacillus amyloliquefaciens* strain A3 also exhibited antibacterial activities [35,38]. Selection of *Bacillus amyloliquefaciens* strain A3 can be used for the production of CFCS and the synthesis of AgNPs, which avoids the screening of bacteria and can be used as a reference strain for the synthesis of AgNPs.

In conclusion, we provide a simple, environmentally safe, and economically viable control strategy to combat the bacterial pathogen *Dickeya dadantii* using a combination of AgNPs and CFCS. *Dickeya dadantii*-infected sweet potato can be treated with the combination of AgNPs (12 µg) and CFCS (12%) to produce a healthy seed crop. This can minimize the labor required to produce a large amount of CFCS and reduce the chance of releasing Ag⁺ from AgNPs. The combination of AgNPs and CFCS acts as a *Dickeya dadantii* inhibitor and growth promoter for the plant. The promising potency of the combination of AgNPs and cell-free culture supernatant can draw immense research interest in the production of green-synthesized nano pesticides.

3. Materials and Methods

3.1. Bacteria

The pathogenic strain CZ1501 of *D. dadantii* was isolated from infected sweet potato stems cultivated in Hangzhou of Zhejiang province, China, and the biocontrol strain *B. amyloliquefaciens* strain A3 isolated from rice seeds [58] were used in this study. Both bacteria were grown in nutrient agar or broth medium consisting of 10 g of tryptone, 2.5 g of glucose, 5 g of NaCl, and 3 g of beef extract with or without 15 g of agar per liter, respectively, at pH 7.0.

3.2. Preparation of CFCS and Synthesis of AgNPs

Bacillus amyloliquefaciens strain A3 was cultured in NA broth at 30 °C for 48 h at 200 rpm. CFCS was prepared with centrifugation at 27,200× *g* for 15 min and then two times filtration with a 0.22 µm millipore filter. A lack of bacterial presence was confirmed by culturing 100 µL CFCS in nutrient agar for 24 h at 30 °C.

To the biosynthesized AgNPs, 35 mL CFCS of *B. amyloliquefaciens* A3 was mixed with 115 mL of a freshly prepared aqueous solution of 3 mM AgNO₃ (Cat. No. 10018461; Sinopharm, Shanghai, China) in a 250 mL Erlenmeyer flask and kept under shaking at 200 rpm and 30 °C for 48 h in dark conditions. Then, 35 mL of nutrient broth and 115 mL of

3 mM AgNO₃ were added together and used as the control. AgNPs synthesis was observed when the solution changed from a light yellow to dark brown color. After adding 2 mL of the dark brown solution with 2 mL of Milli-Q water, the UV-Visible spectra were observed at 1 nm resolution in the range of 200–750 nm using a Shimadzu UV-2550 spectrometer (Shimadzu, Kyoto, Japan). AgNPs were obtained from the dark brown solution with centrifugation at 27,200× *g* for 10 min followed by washing two times with Milli-Q water, after which they were freeze-dried with Alpha 1-2 LD plus (GmbH, Marburg, Germany). The freeze-dried AgNPs were weighed, and a stock solution of 50 mg·mL⁻¹ was prepared by dissolving AgNPs with Milli-Q water.

3.3. Characterization of AgNPs Synthesized with CFCS with *B. amyloliquefaciens*

The functional groups for the biosynthesis and stabilization of AgNPs were confirmed using Fourier transforms infrared (FTIR) spectroscopy. In detail, 1 mg of freeze-dried AgNP powder was mixed with 300 mg KBr, and thin pellets were made using a hydraulic pellet press. FTIR spectrum was documented with an AVATAR 370 FTIR spectrometer (Thermo Nicolet, Madison, WI, USA) in the range between 500 and 4000 cm⁻¹ with a 4 cm⁻¹ resolution. FTIR spectra were interpreted using the table of Bruker infrared (Bruker Optics Inc., Billerica, MA, USA) and the absorption table of Libre Texts infrared spectroscopy (<https://chem.libretexts.org/>) accessed on 8 June 2018.

To observe the AgNP size and morphology, SEM and TEM were used. One drop of the AgNPs solution was applied onto the carbon-coated copper grid and then dried under a mercury lamp. The SU8010 field emission scanning electron microscope (Hitachi, Tokyo, Japan) and a JEM-1230 transmission electron microscope (JEOL, Tokyo, Japan) were used to observe the grid carried in AgNPs. An X-Max N energy dispersive spectrometer (Oxford Instruments, Oxford, UK) was used to detect the silver element in AgNPs at 20 keV.

The X-ray diffraction pattern was used to understand the crystallographic structure of AgNPs. A coated film of freeze-dried AgNP powder was kept on the glass slide and analyzed using a D8 Advance Diffractometer (Bruker, Karlsruhe, Germany) maintaining an operational condition of 40 kV and 40 mA with a Cu-K α radiation ranging from 20° to 80° at the 2 θ angle.

3.4. Experiments on Ag Release

The metal Ag release from the biosynthesized AgNPs was calculated in sterile ddH₂O according to the previously described method [59] with a few modifications. In brief, suspensions were prepared using 25 μ g·mL⁻¹ AgNPs in ddH₂O with three replications, and the pH was adjusted to 7. The suspensions were incubated at 26 ± 2 °C under continuous shaking at 150 rpm. After 2, 4, 8, 16, and 24 h time intervals, 1 mL aliquot was taken from each suspension and centrifuged at 13,000× *g* to discard NPs. The acquired supernatants were digested by applying HClO₄:HNO₃ (1:3), and the Ag content was analyzed using inductively coupled plasma-mass spectrometry (ICP-MS; Optima 8000DV, Pekin-Elmer, Waltham, MA, USA). The quality of the investigative data was ensured by running a standard suspension containing 100 μ g·mL⁻¹ continually in each of the 5 samples.

3.5. Antibacterial Assay

D. dadantii CZ1501 was grown in nutrient broth at 30 °C with shaking at 200 rpm to the mid-exponential phase, and the concentration of bacterial cells was adjusted to about 5 × 10⁸ CFU·mL⁻¹ before use.

Antibacterial activities of AgNPs synthesized with the CFCS of *B. amyloliquefaciens* strain A3, the CFCS of *B. amyloliquefaciens* strain A3, and the combination of AgNPs with CFCS were determined in the nutrient broth. Briefly, 5 mL of nutrient broth was inoculated with 100 μ L *D. dadantii* suspensions and used as the control. AgNPs from *B. amyloliquefaciens* strain A3 were adjusted to concentrations of 12, 25, and 50 μ g·mL⁻¹ by adding nutrient broth. Furthermore, 100 μ L *D. dadantii* suspensions were inoculated into 5 mL of nutrient broth containing AgNPs. *D. dadantii* suspensions (100 μ L), NA broth (2.4 mL), the CFCS of

B. amyloliquefaciens A3 (0.6 mL or 1.25 mL or 2.5 mL), and sterile distilled water (1.9 mL or 1.25 mL or 0 mL) to a total volume of 5 mL were added into a glass tube to obtain final concentrations of 12, 25, and 50% CFCS. *D. dadantii* suspensions (100 μ L), NA broth (2.4 mL), the CFCS of A3 (0.6 mL or 1.25 mL or 2.5 mL), and sterile distilled water (1.9 mL or 1.25 mL or 0 mL) were mixed, and AgNPs were added with nutrient broth consisting of CFCS to obtain concentrations of 12, 25, and 50 μ g \cdot mL⁻¹. The samples were then incubated at 30 °C and 200 rpm for 24 h. After that, the optical density of the samples was measured at 600 nm (OD₆₀₀) using a SpectraMax spectrophotometer (Molecular Devices, Sunnyvale, CA, USA). This experiment was repeated three times with three replications of each treatment.

The effect of 50 μ g \cdot mL⁻¹ synthesized AgNPs from *B. amyloliquefaciens* strain A3, 50% of the CFCS of *B. amyloliquefaciens* strain A3, and the combination of AgNPs (12 μ g \cdot mL⁻¹) and CFCS (12%) on the swimming motility of *D. dadantii* strain CZ1501 was determined with semi-solid nutrient agar [0.3% (*w/v*)]. A plate without AgNPs and CFCS served as the control. AgNPs were added to semisolid nutrient agar [0.3%, *w/v*] to a concentration of 50 μ g \cdot mL⁻¹. Equal amounts of the CFCS of *B. amyloliquefaciens* strain A3 and semisolid nutrient agar [0.6% (*w/v*)] were mixed to obtain a 50% CFCS concentration. AgNPs and CFCS were added to the semi-solid nutrient agar to obtain a final concentration of 12 μ L AgNPs and 12% of CFCS. In the center of each swimming plate, a suspension (5 μ L) of *D. dadantii* was spotted and incubated for 48 h at 30 °C. The diameter of *D. dadantii* colonies was measured. The experiment was repeated three times with three replicates of each treatment.

The inhibition of biofilm formed by *D. dadantii* strain CZ1501 using AgNPs (50 μ g \cdot mL⁻¹) from *B. amyloliquefaciens* strain A3, CFCS of *B. amyloliquefaciens* strain A3 (50%), the combination of AgNPs (12 μ g \cdot mL⁻¹) and CFCS (12%) was determined using the method of crystal violet staining, which was quantified by measuring the absorbance at 590 nm (OD₅₉₀) using a 96-well microtiter plate. AgNPs were added with nutrient broth to obtain a concentration of 50 μ g \cdot mL⁻¹. AgNPs were added with nutrient broth consisting of 12% CFCS to a concentration of 12 μ g \cdot mL⁻¹. An amount of 100 μ L *D. dadantii* suspensions was mixed with 100 μ L of the CFCS of *B. amyloliquefaciens* A3 or nutrient broth composed of 50 μ g \cdot mL⁻¹ AgNPs (100 μ L) or nutrient broth containing 12 μ g \cdot mL⁻¹ AgNPs along with 12% CFCS (100 μ L). The mixtures were independently added to the wells of a 96-well microplate. Furthermore, a 100 μ L of *D. dadantii* suspension added with 100 μ L of distilled water was used as the control, whereas 100 μ L of nutrient broth with 100 μ L of distilled water was used as the blank. The plates were then incubated without shaking at 30 °C for 24 h. The liquid from each well was discarded and gently washed three times using distilled water followed by 1 h of air drying. In addition, 200 μ L crystal violet (1%, *w/v*) was used to stain the bacterial cells that attached to the wells. A thorough washing was performed after incubation for 30 min at room temperature using distilled water. The crystal violet dye in the bacterial cells was dissolved by adding 33% (*v/v*) of 200 μ L acetic acid in each well. The OD value at 590 nm was measured using SpectraMax spectrophotometer (Molecular Device, Sunnyvale, CA, USA). The experiment was repeated three times with six replicates of each treatment.

The effect of AgNPs (50 μ g \cdot mL⁻¹) from *B. amyloliquefaciens* strain A3, the CFCS of *B. amyloliquefaciens* strain A3 (50%), and the combination of AgNPs (12 μ g \cdot mL⁻¹) and CFCS (12%) on in vivo antagonistic actions against *D. dadantii* was assayed with tuber slices of sweet potato. After surface sterilization with 70% (*v/v*) ethanol, the sweet potato tubers were rinsed with sterile distilled water, and 10 mm thick slices were prepared. The tuber slices were kept in a solution containing 50 μ g \cdot mL⁻¹ AgNPs or 50% CFCS or 12 μ g \cdot mL⁻¹ AgNPs along with 12% CFCS for 1 h, and after that, they were air-dried for 1 h in Petri dishes. Then, 5 μ L of *D. dadantii* cell suspension was spotted by puncturing at the center of the slice. The slices were incubated at 30 °C for 24 h. The diameter of the maceration zones created by *D. dadantii* around the punctures was measured. The experiment was repeated three times with three replicates of each treatment.

3.6. Transmission Electron Microscopy

The combined effect of AgNPs and CFCS on the structure of *D. dadantii* cells was determined using TEM. *D. dadantii* suspension alone or *D. dadantii* suspension containing a combination of AgNPs ($12 \mu\text{g}\cdot\text{mL}^{-1}$) and CFCS of *B. amyloliquefaciens* A3 (12%) were incubated at rotary shaking at 200 rpm and 30°C for 4 h. The sample for TEM analysis was prepared followed by harvesting *D. dadantii* cells as described in our previous work [35], and observations were made using the JEM-1230 transmission electron microscope.

3.7. In Planta Assay

An in planta experiment was assayed to evaluate the efficacy of AgNPs ($50 \mu\text{g}\cdot\text{mL}^{-1}$) derived from the CFCS of *B. amyloliquefaciens* strain A3, the CFCS of *B. amyloliquefaciens* strain A3 (50%), and the combination of AgNPs ($12 \mu\text{g}\cdot\text{mL}^{-1}$) and CFCS (12%) for the growth promotion of sweet potato seedlings and the suppression of *D. dadantii* according to the method of [37] with slight modifications. In brief, after surface sterilization with 70% (*v/v*) ethanol, the sweet potato tubers were rinsed with sterile distilled water and immersed in *D. dadantii* suspension (1×10^7 CFU mL^{-1}) or in sterile distilled water for 4 h. The seed tubers were air dried for 12 h and then immersed in sterile distilled water or AgNPs ($50 \mu\text{g}\cdot\text{mL}^{-1}$) from *B. amyloliquefaciens* strain A3, *B. amyloliquefaciens* strain A3-originated CFCS (50%), or the combination of AgNPs ($12 \mu\text{g}\cdot\text{mL}^{-1}$) and CFCS (12%) for 4 h. After treatment, all seed tubers were kept on three-layered moistened and sterilized filter papers in Petri dishes of 15 cm diameter. A single seed tuber was placed in a petri dish and was kept in a growth chamber for 21 days, maintaining 28°C temperature, 80% humidity, and a 12/12-h light/dark photoperiod. After 21 days of incubation, seedling height was measured. The experiment was repeated three times with six replications of each treatment.

3.8. Statistical Analysis

Experimental data were analyzed using SPSS software version 16 (SPSS, Chicago, IL, USA) at a $p < 0.05$ level of significance. All data are presented as the mean of at least three values with their standard error for each independent experiment.

Author Contributions: Conceptualization, A.H., M.A.A. and B.L.; methodology, A.H.; software, T.A. and M.S.; validation, A.H., M.M.H., R.H.K., T.A., M.S., Q.A. and Y.W.; formal analysis, M.A.A.; investigation, J.L. and R.C.; resources, J.L., R.C., M.M.H. and R.H.K.; data curation, T.A.; writing—original draft preparation, A.H.; writing—review and editing, T.A.; visualization, R.H.K.; supervision, J.L., Q.A. and Y.W.; project administration, Y.W.; funding acquisition, M.M.H. and Y.W. All authors have read and agreed to the published version of the manuscript.

Funding: Funding was provided by the Shanghai Agriculture Applied Technology Development Program (2021-02-08-00-12-F00771), the Hangzhou Science and Technology Development Plan Project (202003A05), the Zhejiang Provincial Key R & D Program of China (2017C02002), and the State Key Laboratory for Managing Biotic and Chemical Threats to the Quality and Safety of Agro-products (2010DS700124-ZZ2014; 2010DS700124-KF202101; 2010DS700124-KF202205).

Data Availability Statement: The data is contained within the manuscript.

Acknowledgments: The authors extend their appreciation to “Taif University for supporting current work by Taif University Researchers Supporting Project number (TURSP—2020/59), Taif University, Taif, Saudi Arabia”.

Conflicts of Interest: The authors declare no conflict of interest.

References

1. Abbas, Q.; Liu, G.; Yousaf, B.; Ali, M.U.; Ullah, H.; Ahmed, R. Effects of biochar on uptake, acquisition and translocation of silver nanoparticles in rice (*Oryza sativa* L.) in relation to growth, photosynthetic traits and nutrients displacement. *Environ. Pollut.* **2019**, *250*, 728–736. [[CrossRef](#)] [[PubMed](#)]
2. Tangaa, S.R.; Selck, H.; Winther-Nielsen, M.; Khan, F.R. Trophic transfer of metal-based nanoparticles in aquatic environments: A review and recommendations for future research focus. *Environ. Sci. Nano* **2016**, *3*, 966–981. [[CrossRef](#)]

3. Ahmed, S.; Ahmad, M.; Swami, B.L.; Ikram, S. A review on plants extract mediated synthesis of silver nanoparticles for antimicrobial applications: A green expertise. *J. Adv. Res.* **2016**, *7*, 17–28. [[CrossRef](#)] [[PubMed](#)]
4. Guzman, M.; Dille, J.; Godet, S. Synthesis and antibacterial activity of silver nanoparticles against gram-positive and gram-negative bacteria. *Nanomed. Nanotechnol. Biol. Med.* **2012**, *8*, 37–45. [[CrossRef](#)] [[PubMed](#)]
5. Sharma, V.K.; Yngard, R.A.; Lin, Y. Silver nanoparticles: Green synthesis and their antimicrobial activities. *Adv. Colloid Interface Sci.* **2009**, *145*, 83–96. [[CrossRef](#)]
6. Gudkov, S.V.; Serov, D.A.; Astashev, M.E.; Semenova, A.A.; Lisitsyn, A.B. Ag₂O nanoparticles as a candidate for antimicrobial compounds of the new generation. *Pharmaceuticals* **2022**, *15*, 968. [[CrossRef](#)]
7. Franci, G.; Falanga, A.; Galdiero, S.; Palomba, L.; Rai, M.; Morelli, G.; Galdiero, M. Silver nanoparticles as potential antibacterial agents. *Molecules* **2015**, *20*, 8856–8874. [[CrossRef](#)]
8. Devatha, C.P.; Thalla, A.K. Green synthesis of nanomaterials. In *Synthesis of Inorganic Nanomaterials*; Elsevier: Amsterdam, The Netherlands, 2018; pp. 169–184.
9. Khan, T.; Jalal, H.; Karam, K.; Khan, M.A. Biodegradable gum: A green source for silver nanoparticles. In *Green Synthesis of Silver Nanomaterials*; Elsevier: Amsterdam, The Netherlands, 2022; pp. 189–217.
10. Cvjetko, P.; Milošić, A.; Domijan, A.-M.; Vrček, I.V.; Tolić, S.; Štefanić, P.P.; Letofsky-Papst, I.; Tkalec, M.; Balen, B. Toxicity of silver ions and differently coated silver nanoparticles in *Allium cepa* roots. *Ecotoxicol. Environ. Saf.* **2017**, *137*, 18–28. [[CrossRef](#)]
11. Vishwakarma, K.; Upadhyay, N.; Singh, J.; Liu, S.; Singh, V.P.; Prasad, S.M.; Chauhan, D.K.; Tripathi, D.K.; Sharma, S. Differential phytotoxic impact of plant mediated silver nanoparticles (AgNPs) and silver nitrate (AgNO₃) on *Brassica* sp. *Front. Plant Sci.* **2017**, *8*, 1501. [[CrossRef](#)]
12. Lastochkina, O.; Seifikalhor, M.; Aliniaiefard, S.; Baymiev, A.; Pusenkova, L.; Garipova, S.; Kulabuhova, D.; Maksimov, I. *Bacillus* spp.: Efficient biotic strategy to control postharvest diseases of fruits and vegetables. *Plants* **2019**, *8*, 97. [[CrossRef](#)]
13. Shafi, J.; Tian, H.; Ji, M. *Bacillus* species as versatile weapons for plant pathogens: A review. *Biotechnol. Biotechnol. Equip.* **2017**, *31*, 446–459. [[CrossRef](#)]
14. Ongena, M.; Jacques, P. *Bacillus* lipopeptides: Versatile weapons for plant disease biocontrol. *Trends Microbiol.* **2008**, *16*, 115–125. [[CrossRef](#)]
15. Fira, D.; Dimkić, I.; Berić, T.; Lozo, J.; Stanković, S. Biological control of plant pathogens by *Bacillus* species. *J. Biotechnol.* **2018**, *285*, 44–55. [[CrossRef](#)]
16. Wu, L.; Wu, H.; Chen, L.; Yu, X.; Borriss, R.; Gao, X. Difficidin and bacilysin from *Bacillus amyloliquefaciens* FZB42 have antibacterial activity against *Xanthomonas oryzae* rice pathogens. *Sci. Rep.* **2015**, *5*, 12975. [[CrossRef](#)]
17. Yoshida, S.; Hiradate, S.; Tsukamoto, T.; Hatakeda, K.; Shirata, A. Antimicrobial activity of culture filtrate of *Bacillus amyloliquefaciens* RC-2 isolated from mulberry leaves. *Phytopathology* **2001**, *91*, 181–187. [[CrossRef](#)]
18. Derbalah, A.S.; Elkot, G.A.E.; Hamza, A.M. Laboratory evaluation of botanical extracts, microbial culture filtrates and silver nanoparticles against *Botrytis cinerea*. *Ann. Microbiol.* **2012**, *62*, 1331–1337. [[CrossRef](#)]
19. Abbas, A.; Khan, S.U.; Khan, W.U.; Saleh, T.A.; Khan, M.H.U.; Ullah, S.; Ali, A.; Ikram, M. Antagonist effects of strains of *Bacillus* spp. against *Rhizoctonia solani* for their protection against several plant diseases: Alternatives to chemical pesticides. *Comptes Rendus Biol.* **2019**, *342*, 124–135. [[CrossRef](#)]
20. Adeolu, M.; Alnajjar, S.; Naushad, S.; Gupta, R.S. Genome-based phylogeny and taxonomy of the ‘*Enterobacteriales*’: Proposal for *Enterobacterales* ord. nov. divided into the families *Enterobacteriaceae*, *Erwiniaceae* fam. nov., *Pectobacteriaceae* fam. nov., *Yersiniaceae* fam. nov., *Hafniaceae* fam. nov., *Morganellaceae* fam. nov., and *Budviciaceae* fam. nov. *Int. J. Syst. Evol. Microbiol.* **2016**, *66*, 5575–5599.
21. Ma, B.; Hibbing, M.E.; Kim, H.-S.; Reedy, R.M.; Yedidia, I.; Breuer, J.; Breuer, J.; Glasner, J.D.; Perna, N.T.; Kelman, A. Host range and molecular phylogenies of the soft rot enterobacterial genera *Pectobacterium* and *Dickeya*. *Phytopathology* **2007**, *97*, 1150–1163. [[CrossRef](#)]
22. Charkowski, A.O. The changing face of bacterial soft-rot diseases. *Annu. Rev. Phytopathol.* **2018**, *56*, 269–288. [[CrossRef](#)]
23. Czajkowski, R.; Perombelon, M.C.; van Veen, J.A.; van der Wolf, J.M. Control of blackleg and tuber soft rot of potato caused by *Pectobacterium* and *Dickeya* species: A review. *Plant Pathol.* **2011**, *60*, 999–1013. [[CrossRef](#)]
24. Liu, Q.; Zeng, X.; Li, B. Pathogen identification of a new bacterial rice foot rot disease in Guangdong province. *J. South China Agric. Univ.* **1997**, *18*, 128–129.
25. Pu, X.; Zhou, J.; Lin, B.; Shen, H. First report of bacterial foot rot of rice caused by a *Dickeya zeae* in China. *Plant Dis.* **2012**, *96*, 1818. [[CrossRef](#)] [[PubMed](#)]
26. Kumar, A.; Hunjan, M.S.; Kaur, H.; Rawal, R.; Kumar, A.; Singh, P. A review on bacterial stalk rot disease of maize caused by *Dickeya zeae*. *J. Appl. Nat. Sci.* **2017**, *9*, 1214–1225. [[CrossRef](#)]
27. Jiang, H.; Hao, J.; Johnson, S.; Brueggeman, R.; Secor, G. First report of *Dickeya dianthicola* causing blackleg and bacterial soft rot on potato in Maine. *Plant Dis.* **2016**, *100*, 2320. [[CrossRef](#)]
28. McNally, R.; Curland, R.; Webster, B.; Robinson, A.; Ishimaru, C. First report of stem rot on potato caused by *Dickeya chrysanthemi* in Minnesota. *Plant Dis.* **2018**, *102*, 238. [[CrossRef](#)]
29. Toth, I.; Van Der Wolf, J.; Saddler, G.; Lojkowska, E.; Hélias, V.; Pirhonen, M.; Tsrör, L.; Elphinstone, J. *Dickeya* species: An emerging problem for potato production in Europe. *Plant Pathol.* **2011**, *60*, 385–399. [[CrossRef](#)]

30. Huang, L.; Fang, B.; Luo, Z.; Chen, J.; Zhang, X.; Wang, Z. First report of bacterial stem and root rot of sweetpotato caused by a *Dickeya* sp. (*Erwinia chrysanthemi*) in China. *Plant Dis.* **2010**, *94*, 1503. [[CrossRef](#)]
31. Shen, X.; Lin, C.; Qian, J.; Qiu, Z.; Chen, J.; Sun, C.; Yi, J.; Lou, B. Characterization of stem and root rot symptoms of sweet potato and the causal pathogen of the disease. *Acta Phytopathol. Sin* **2018**, *48*, 25–34.
32. Liu, Q.; Xiao, W.; Wu, Z.; Li, S.; Yuan, Y.; Li, H. Identification of *Dickeya dadantii* as a causal agent of banana bacterial sheath rot in China. *J. Plant Pathol.* **2016**, 503–510.
33. Zhang, J.; Shen, H.; Pu, X.; Lin, B.; Hu, J. Identification of *Dickeya zeae* as a causal agent of bacterial soft rot in banana in China. *Plant Dis.* **2014**, *98*, 436–442. [[CrossRef](#)]
34. Hossain, A.; Abdallah, Y.; Ali, M.; Masum, M.; Islam, M.; Li, B.; Sun, G.; Meng, Y.; Wang, Y.; An, Q. Lemon-fruit-based green synthesis of zinc oxide nanoparticles and titanium dioxide nanoparticles against soft rot bacterial pathogen *Dickeya dadantii*. *Biomolecules* **2019**, *9*, 863. [[CrossRef](#)]
35. Hossain, A.; Hong, X.; Ibrahim, E.; Li, B.; Sun, G.; Meng, Y.; Wang, Y.; An, Q. Green Synthesis of Silver Nanoparticles with Culture Supernatant of a Bacterium *Pseudomonas rhodesiae* and Their Antibacterial Activity against Soft Rot Pathogen *Dickeya dadantii*. *Molecules* **2019**, *24*, 2303. [[CrossRef](#)]
36. Hossain, A.; Ali, M.A.; Lin, L.; Luo, J.; You, Y.; Masum, M.M.I.; Jiang, Y.; Wang, Y.; Li, B.; An, Q. Biocontrol of Soft Rot *Dickeya* and *Pectobacterium* Pathogens by Broad-Spectrum Antagonistic Bacteria within *Paenibacillus polymyxa* Complex. *Microorganisms* **2023**, *11*, 817. [[CrossRef](#)]
37. Hossain, A.; Islam Masum, M.M.; Wu, X.; Abdallah, Y.; Ogunyemi, S.O.; Wang, Y.; Sun, G.; Li, B.; An, Q. Screening of *Bacillus* strains in biocontrol of pathogen *Dickeya dadantii* causing stem and root rot disease of sweet potato. *Biocontrol Sci. Technol.* **2020**, *30*, 1180–1198. [[CrossRef](#)]
38. Fouad, H.; Hongjie, L.; Yanmei, D.; Baoting, Y.; El-Shakh, A.; Abbas, G.; Jianchu, M. Synthesis and characterization of silver nanoparticles using *Bacillus amyloliquefaciens* and *Bacillus subtilis* to control filarial vector *Culex pipiens pallens* and its antimicrobial activity. *Artif. Cells Nanomed. Biotechnol.* **2017**, *45*, 1369–1378. [[CrossRef](#)]
39. Mulvaney, P. Surface plasmon spectroscopy of nanosized metal particles. *Langmuir* **1996**, *12*, 788–800. [[CrossRef](#)]
40. Anthony, K.J.P.; Murugan, M.; Gurunathan, S. Biosynthesis of silver nanoparticles from the culture supernatant of *Bacillus marisflavi* and their potential antibacterial activity. *J. Ind. Eng. Chem.* **2014**, *20*, 1505–1510. [[CrossRef](#)]
41. Elbeshehy, E.K.; Elazzazy, A.M.; Aggelis, G. Silver nanoparticles synthesis mediated by new isolates of *Bacillus* spp., nanoparticle characterization and their activity against Bean Yellow Mosaic Virus and human pathogens. *Front. Microbiol.* **2015**, *6*, 453. [[CrossRef](#)]
42. Padman, A.J.; Henderson, J.; Hodgson, S.; Rahman, P.K. Biomediated synthesis of silver nanoparticles using *Exiguobacterium mexicanum*. *Biotechnol. Lett.* **2014**, *36*, 2079–2084. [[CrossRef](#)]
43. Kumar, C.G.; Mamidyala, S.K. Extracellular synthesis of silver nanoparticles using culture supernatant of *Pseudomonas aeruginosa*. *Colloids Surf. B Biointerfaces* **2011**, *84*, 462–466. [[CrossRef](#)] [[PubMed](#)]
44. Momin, B.; Rahman, S.; Jha, N.; Annapure, U.S. Valorization of mutant *Bacillus licheniformis* M09 supernatant for green synthesis of silver nanoparticles: Photocatalytic dye degradation, antibacterial activity, and cytotoxicity. *Bioprocess Biosyst. Eng.* **2019**, *42*, 541–553. [[CrossRef](#)] [[PubMed](#)]
45. Singh, H.; Du, J.; Singh, P.; Yi, T.H. Extracellular synthesis of silver nanoparticles by *Pseudomonas* sp. THG-LS1. 4 and their antimicrobial application. *J. Pharm. Anal.* **2018**, *8*, 258–264. [[CrossRef](#)] [[PubMed](#)]
46. Banasiuk, R.; Krychowiak, M.; Swigon, D.; Tomaszewicz, W.; Michalak, A.; Chylewska, A.; Ziabka, M.; Lapinski, M.; Koscielska, B.; Narajczyk, M. Carnivorous plants used for green synthesis of silver nanoparticles with broad-spectrum antimicrobial activity. *Arab. J. Chem.* **2020**, *13*, 1415–1428. [[CrossRef](#)]
47. Kalimuthu, K.; Babu, R.S.; Venkataraman, D.; Bilal, M.; Gurunathan, S. Biosynthesis of silver nanocrystals by *Bacillus licheniformis*. *Colloids Surf. B Biointerfaces* **2008**, *65*, 150–153. [[CrossRef](#)]
48. Velmurugan, P.; Iydroose, M.; Mohideen, M.H.A.K.; Mohan, T.S.; Cho, M.; Oh, B.-T. Biosynthesis of silver nanoparticles using *Bacillus subtilis* EWP-46 cell-free extract and evaluation of its antibacterial activity. *Bioprocess Biosyst. Eng.* **2014**, *37*, 1527–1534. [[CrossRef](#)]
49. Shao, W.; Liu, X.; Min, H.; Dong, G.; Feng, Q.; Zuo, S. Preparation, characterization, and antibacterial activity of silver nanoparticle-decorated graphene oxide nanocomposite. *ACS Appl. Mater. Interfaces* **2015**, *7*, 6966–6973. [[CrossRef](#)]
50. Xiu, Z.-m.; Zhang, Q.-b.; Puppala, H.L.; Colvin, V.L.; Alvarez, P.J. Negligible particle-specific antibacterial activity of silver nanoparticles. *Nano Lett.* **2012**, *12*, 4271–4275. [[CrossRef](#)]
51. Ivask, A.; ElBadawy, A.; Kaweteerawat, C.; Boren, D.; Fischer, H.; Ji, Z.; Chang, C.H.; Liu, R.; Tolaymat, T.; Telesca, D. Toxicity mechanisms in *Escherichia coli* vary for silver nanoparticles and differ from ionic silver. *ACS Nano* **2014**, *8*, 374–386. [[CrossRef](#)]
52. Ivask, A.; Kurvet, I.; Kasemets, K.; Blinova, I.; Aruoja, V.; Suppi, S.; Vija, H.; Käkinen, A.; Titma, T.; Heinlaan, M. Size-dependent toxicity of silver nanoparticles to bacteria, yeast, algae, crustaceans and mammalian cells in vitro. *PLoS ONE* **2014**, *9*, e102108. [[CrossRef](#)]
53. Zawadzka, K.; Kądziola, K.; Felczak, A.; Wrońska, N.; Piwoński, I.; Kisiełowska, A.; Lisowska, K. Surface area or diameter—which factor really determines the antibacterial activity of silver nanoparticles grown on TiO₂ coatings? *New J. Chem.* **2014**, *38*, 3275–3281. [[CrossRef](#)]

54. Durán, N.; Durán, M.; de Jesus, M.B.; Seabra, A.B.; Fávaro, W.J.; Nakazato, G. Silver nanoparticles: A new view on mechanistic aspects on antimicrobial activity. *Nanomed. Nanotechnol. Biol. Med.* **2016**, *12*, 789–799. [[CrossRef](#)]
55. Chen, X.; Koumoutsis, A.; Scholz, R.; Schneider, K.; Vater, J.; Süßmuth, R.; Piel, J.; Borriss, R. Genome analysis of *Bacillus amyloliquefaciens* FZB42 reveals its potential for biocontrol of plant pathogens. *J. Biotechnol.* **2009**, *140*, 27–37. [[CrossRef](#)] [[PubMed](#)]
56. Rückert, C.; Blom, J.; Chen, X.; Reva, O.; Borriss, R. Genome sequence of *B. amyloliquefaciens* type strain DSM7T reveals differences to plant-associated *B. amyloliquefaciens* FZB42. *J. Biotechnol.* **2011**, *155*, 78–85. [[CrossRef](#)]
57. Mnif, I.; Ghribi, D. Review lipopeptides biosurfactants: Mean classes and new insights for industrial, biomedical, and environmental applications. *Pept. Sci.* **2015**, *104*, 129–147. [[CrossRef](#)]
58. El-shakh, A.S.; Kakar, K.U.; Wang, X.; Almoneafy, A.A.; Ojaghian, M.R.; Li, B.; Anjum, S.I.; Xie, G.-l. Controlling bacterial leaf blight of rice and enhancing the plant growth with endophytic and rhizobacterial *Bacillus* strains. *Toxicol. Environ. Chem.* **2015**, *97*, 766–785. [[CrossRef](#)]
59. Abbas, Q.; Yousaf, B.; Ullah, H.; Ali, M.U.; Zia-ur-Rehman, M.; Rizwan, M.; Rinklebe, J. Biochar-induced immobilization and transformation of silver-nanoparticles affect growth, intracellular-radicles generation and nutrients assimilation by reducing oxidative stress in maize. *J. Hazard. Mater.* **2020**, *390*, 121976. [[CrossRef](#)]

Disclaimer/Publisher’s Note: The statements, opinions and data contained in all publications are solely those of the individual author(s) and contributor(s) and not of MDPI and/or the editor(s). MDPI and/or the editor(s) disclaim responsibility for any injury to people or property resulting from any ideas, methods, instructions or products referred to in the content.